Dual-rotor tool path generation and removal error analysis in active feed polishing

Shaozhi Wang,* Jian Liu, and Linghua Zhang

The State Key Laboratory of Applied Optics, Changchun Institute of Optics, Fine Mechanics and Physics, Chinese Academy of Science, Changchun 130033, China

*Corresponding author: shaozhi137@163.com

Received 10 June 2013; revised 30 August 2013; accepted 31 August 2013; posted 4 September 2013 (Doc. ID 191952); published 30 September 2013

High-quality ultrasmooth surface is needed in modern optics, while the existing ultrasmooth surface processing methods are difficult to meet the requirement of the surface figure. In order to solve this problem, the active feed polishing (AFP) is taken as the research object, and the dual-rotor tool path is put forward for this technology. This tool path is generated based on the motion synthesis principle, which realizes smooth connection between different sections. At the same time, the eccentricity, the speed ratio, the velocity, and other parameters can be modified easily, avoiding using the complicated dual-rotor polishing mechanism. In order to further analyze the removal error, the removal amount calculation method for the dual-rotor path is researched and proposed. The simulation analysis results show that the greatest influence factor for the removal error is the sampling interval, the influence of the eccentricity and the speed ratio is less, and the velocity has little impact on it. In addition, the removal error can be controlled within acceptable range by reasonable selection of process parameters. Finally, through a processing experiment of a 100 mm plane lens, the feasibility and effectiveness of this path is verified. This experimental result shows that the AFP technology using the dual-rotor tool path can effectively correct the surface shape while reducing the surface roughness.

OCIS codes: (220.0220) Optical design and fabrication; (220.4610) Optical fabrication.
http://dx.doi.org/10.1364/AO.52.006948

1. Introduction

Modern science and technique put forward a higher requirement for optical surface quality, so ultrasmooth fabrication technology becomes an important research direction because it can get extremely low surface roughness. At present, the common ultrasmooth processing methods include float polishing (FP) [1,2], bowl polishing [3], elastic emission machining (EEM) [4–6], chemical mechanical polishing [7,8], and plasma-assisted chemical etching [9]. However, most of these methods process the whole surface simultaneously, so that it is difficult for them to balance the surface figure. In theory, the EEM can correct the surface figure during ultrasmooth processing, but the efficiency is slow. So, it becomes an urgent problem to search a processing method that can balance surface roughness and figure.

Active feed polishing (AFP) technology is a new kind of ultrasmooth processing method that is proposed on the basis of FP principle combined with small tool polishing. The small tool polishing [10] not only has a high efficiency, but also provides a possibility that the surface figure and roughness can be balanced at the same time. The AFP technology will be studied in how to correct the surface figure during the ultrasmooth processing, and the motion mode and removal error will be analyzed too.

2. Basic Theories

The principle of the AFP technology is shown in Fig. 1. The slurry is supplied from the center of the polishing head and flows through the microholes

1559-128X/13/286948-08$15.00/0

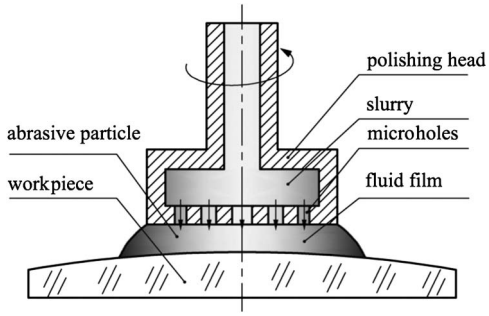

Fig. 1. Schematic of the polishing head of AFP.

at the bottom. In the polishing process, the polishing head is rotating so that the load between the pad and workpiece is supported by a fluid layer [11,12]. At this time, the slurry in this layer moves along the circumferential direction. And the microabrasive in the slurry scratch the surface along the tangential direction by a large speed, to finally remove the surface atoms. So it can obtain the ultrasmooth surface without bringing subsurface damage. Furthermore, some factors require adjustment, such as slurry properties, processing time and rotating speed, so that enough shear force can be generated to remove the material. In addition, spherical and aspherical optical elements can be also processed by controlling the position and angle of the polishing head.

Although the AFP is developed based on the principle of FP, its essence is small tool polishing, so the theory of small tool polishing is also suitable for it. In the description of small tool polishing theory, there are two important equations, one is to describe the removal amount, which was proposed by Preston [13] in 1927

$$\Delta h(x,y) = k \cdot v(x,y) \cdot p(x,y), \tag{1}$$

where $\Delta h(x,y)$, $v(x,y)$ and $p(x,y)$ is the unit time removal amount, instantaneous relative velocity, and instantaneous pressure at point (x,y). k is the proportional coefficient that is related to the polishing conditions. This equation points out that the removal rate is proportional to the relative velocity and pressure. In the AFP, the slurry under the polishing head updates fast and it is well-distributed due to the array of microholes, so the uniformity under the polishing head is superior to an ordinary polishing head, and more suitable for application of the Preston equation.

Another equation describes the processing of small tool polishing:

$$W(x,y) = R(x,y) ** T(x,y), \tag{2}$$

where $W(x,y)$, $R(x,y)$, and $T(x,y)$ denote, respectively, the removal amount, removal function, and dwell time function, $**$ means two-dimensional convolution. The equation shows that the removal amount is equal to the convolution of the removal function to the dwell time in the trajectory [14].

As can be seen, the removal function is the basic function to describe the polishing characteristics. In 1977, Jones proposed that the optimum tool removal profile is to have a central peak and a fairly rapid decrease to zero, and a good method for generating it was dual-rotations [14]. That means the polishing tool has orbital and spin motion simultaneously. The principle of the dual-rotations mechanism is shown in Fig. 2. According to this principle, Jones designed the first computer-controlled polishing machine in the world, which reached a great success [15–17]. From then on, this kind of dual-rotor tool was widely adopted in computer controlled optical surfacing (CCOS), and therefore CCOS is widely used even in complex optical surfaces, such as meter-class optics, segmented mirrors, off-axis mirrors, and so forth [18–21].

This way is effective in the practice, but it also is inconvenient for mechanical design. Literature [18,22,23] use the planetary mechanism to realize the planet movement, but this type of transmission chain is complex, and not conductive to adjusting the speed ratio and eccentricity. For the AFP, it is difficult to supply the slurry inside the polishing head. If the planetary mechanism is added, the system will become cumbersome and extremely complicated. In order to realize planet movement and avoid using the dual-rotor polishing mechanism, the principle of motion synthesis is used, and the related problems will be studied in later sections.

3. Dual-Rotor Tool Path Generation and Error Analysis

A. Basic Principle of Dual-Rotor Tool Path Generation

The motion principle of the existing dual-rotor polishing mechanism is shown in Fig. 3(a). The polishing pad whose radius is r_2 rotates with the spin angular velocity w_2. At the same time, it revolves around the orbital axis o_1 with the orbital angular velocity w_1, and the orbital radius is r_1. That constitutes the motion mode of the dual-rotor polishing mechanism. In the polishing process, the orbital and the spin motion are completed by the dual-rotor mechanism, which is driven by machine to move

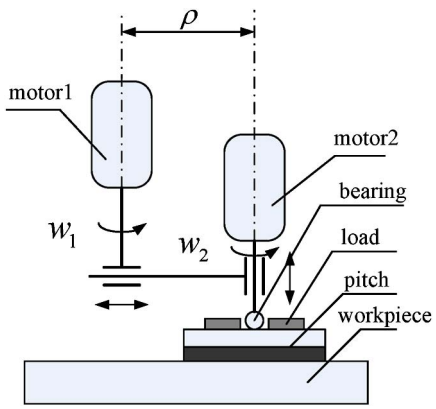

Fig. 2. Dual-rotor polishing mechanism.

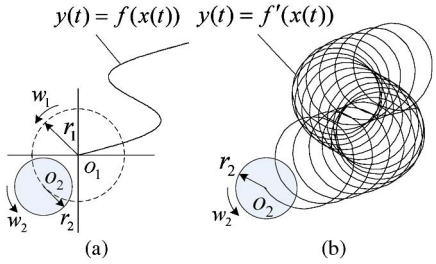

Fig. 3. Motion trajectory of dual-rotor polishing head. (a) Dual-rotor mechanism and (b) dual-rotor path.

along a certain function curve $f(x(t))$ to finish the whole surface processing.

The path of motion synthesis mode is shown in Fig. 3(b), which can be called the dual-rotor tool path. In this movement, the polishing pad only completes spin motion. The orbital and translational motion is all completed by machine X–Y axis. That is to say, the trajectory of the polishing pad $f'(x(t))$ is the synthesis motion of orbital and translational motion. And this synthesis motion can be realized by moving the X–Y axis of the machine under the control of the computer. This kind of method cannot only simulate the trajectory of the dual-rotor polishing mechanism, but also greatly simplifies the mechanical design. In addition, it is convenient to modify the parameters online, such as speed ratio and eccentricity.

The key of the motion synthesis is to get the moving path of the center of the polishing head, which can be describes as

$$\begin{aligned} x(t) &= r_1 \cdot \cos(w_1 * t) + \varphi(t) \\ y(t) &= \underbrace{r_1 \cdot \sin(w_1 * t)}_{1} + \underbrace{\psi(t)}_{2}, \end{aligned} \tag{3}$$

where the first part describes the orbital motion of the polishing head, the second part describes the translation motion. This formula represents the general circumstance.

After identifying the basic form of the path, it also needs to join the path of different sections smoothly. Considering the raster scanning path is often used in actual processing, the workpiece surface can be first divided into a homogeneous rectangular grid and then two adjacent points are selected to study the connection of two paths, as shown in Fig. 4, where N_i, N_{i+1} are two adjacent points in one rectangular grid, m_i is the middle point of N_i and N_{i+1}.

In theory, the dwell time at each grid point can be calculated accurately, but actually, the polishing head cannot only stay at the grid point. The common situation is that the polishing head is controlled to move continuously near the grid point, to make the residence time equal to the theory dwell time of the grid point.

In Fig. 4, the adjacent area of the point N_i is the region between m_{i-1} and m_i, the adjacent area of N_{i+1} is between m_i and m_{i+1}. The spiral line represents the trajectory of the center of the polishing head. The dwell time of point N_i is T_i; similarly, the dwell time of point N_{i+1} is T_{i+1}.

At a certain time, the orbital center of the polishing head moves to point m_i, and the center of the polishing head moves to point P. If the phase of the point P relative to point m_i is taken as the initial phase of section N_{i+1}, the continuity of the phase at different sections can be ensured, that is,

$$\begin{aligned} x_{i+1}(t) &= r_1 \cdot \cos(w_1 * t + \theta_i) + k_{i+1} * t \\ y_{i+1}(t) &= r_1 \cdot \sin(w_1 * t + \theta_i), \end{aligned} \tag{4}$$

where θ_i represents the spiral phase at the end of section N_i.

This cannot only ensure the continuity of the path, but also ensure the continuity of the velocity direction, to make the machine move smoothly during processing.

B. Removal Amount Calculation of the Dual-Rotor Tool Path

Considering the raster scanning path is usually used in the processing, the only situation that will be studied is when the center of the dual-rotor moves along a straight line, as shown in Fig. 5.

In the figure, O_2 is the center of the polishing head, O_1 is the instantaneous orbital center of the polishing head. r_2 represents the radius of the polishing head, r_1 represents the instantaneous orbital radius of the polishing head. w_1 and w_2 represent the angular velocity of orbital and spin motion.

According to above analysis, the synthesis motion of the center of the polishing head can be expressed as

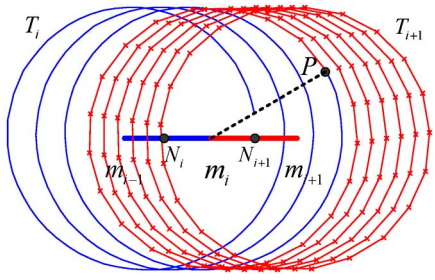

Fig. 4. Connection of different sections in dual-rotor tool path.

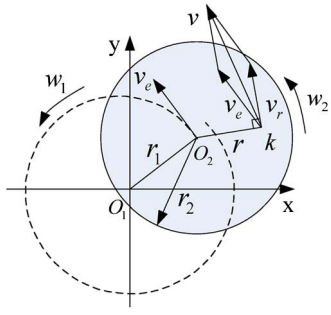

Fig. 5. Motion analysis diagram of the dual-rotor tool path.

$$\begin{cases} x = r_1 \cdot \cos(w_1 t) + k_1 \cdot t \\ y = r_1 \cdot \sin(w_1 t) + k_2 \cdot t \end{cases}. \tag{5}$$

After derivation, the velocity of the center of the polishing head can be obtained as

$$\begin{cases} x' = -r_1 \cdot w_1 \sin(w_1 t) + k_1 \\ y' = r_1 \cdot w_1 \cos(w_1 t) + k_2 \end{cases}. \tag{6}$$

Suppose that sometime a point P on the workpiece has a distance of r with the center of the polishing head, and the coincidence point with P on the polishing head is k. From the theory of mechanics, the velocity of point k is the synthesis vector of following velocity and relative velocity. Known from Fig. 5, the magnitude and direction of the following velocity is

$$\begin{cases} v_e = \sqrt{x'^2 + y'^2} \\ \theta_e = \arctan\left(\frac{y'}{x'}\right) \end{cases}. \tag{7}$$

The relative velocity's magnitude and direction is

$$\begin{cases} v_r = r \cdot w_2 \\ \theta_r = \pi - w_2 t \end{cases}, \tag{8}$$

where r is the distance between k and O_2, and it can be calculated as

$$r = \sqrt{r_x^2 + r_y^2} = \sqrt{(k_x - O_{2x})^2 + (k_y - O_{2y})^2}. \tag{9}$$

So the synthesis speed of point k is

$$\begin{cases} v_x = v_e \cdot \cos\theta_e + v_r \cdot \cos\theta_r \\ v_y = v_e \cdot \sin\theta_e + v_r \cdot \sin\theta_r \end{cases}, \tag{10}$$

$$v = \sqrt{v_x^2 + v_y^2}. \tag{11}$$

Because all the variables eventually come down to the function of t, the final removal rate of the dual-rotor tool path is

$$H(t) = KP \int_0^t v(t)\mathrm{d}t. \tag{12}$$

Through the simulation, the theoretical removal function and the dual-rotor path removal shape can be obtained, as shown in Fig. 6.

In Fig. 6, the eccentricity e of the dual-rotor is 0.8, the speed ratio n is 8. In order to compare them clearly, the axis unit of Fig. 6(a) is normalized, and the axis unit of Fig. 6(b) is reduced in the same scale. As can be seen, the removal shape of the dual-rotor path is significantly elongated and the highest point is lower than the theoretical removal function.

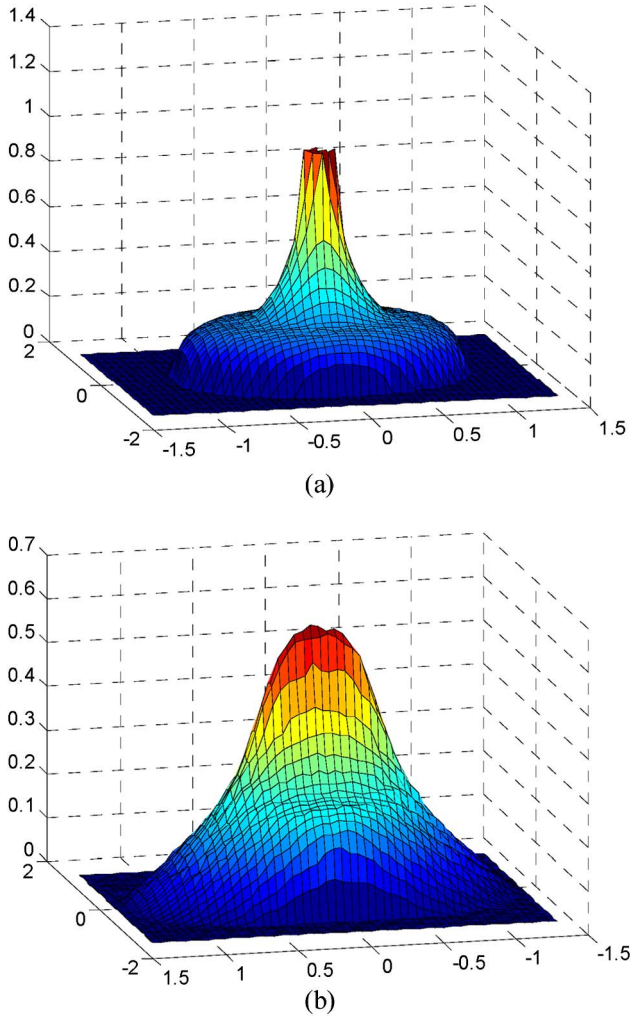

Fig. 6. Comparison between the theoretical removal function and the dual-rotor path removal shape. (a) Theoretical removal function and (b) dual-rotor path removal shape.

C. Removal Error Analysis of the Dual-Rotor Tool Path

In order to analyze the influence of the polishing parameters on the removal function, the removal error of the dual-rotor tool path can be first defined as

$$\delta = \frac{\int_{i \in S} \zeta_i}{\int_{j \in R} R_j}. \tag{13}$$

It can be explained with Fig. 7. S is a large enough space that contains theoretical and actual removal range. At point i, the removal amount of the

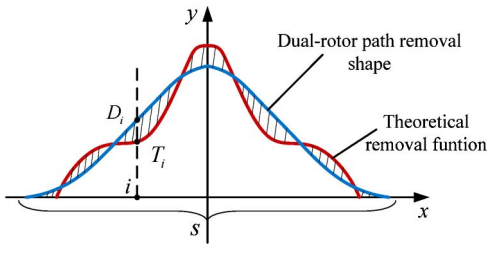

Fig. 7. Profile figure for removal error analysis.

theoretical removal function is T_i, the removal amount of the dual-rotor path removal shape is D_i. ζ_i is the removal amount deviation between theory and practice, so $\zeta_i = |D_i - T_i|$, which is expressed in the form of absolute value. And the $\int_{i\in S} \zeta_i$ means the part in shade. R_j means the theory removal amount in point j. R is the theory removal range.

Three key factors will be considered to analyze the removal error of the dual-rotor tool path.

1. *Influence of Sampling Interval*

In order to unify the effects of different polishing head diameters, define the relative sampling interval as

$$L' = \frac{L}{D}, \tag{14}$$

where L is the sampling interval, D is the diameter of the removal function.

When the sampling interval is larger, the actual removal shape will be "stretched" than the theoretical removal function and finally brings error. The relationship between L' and δ can be researched under different eccentricity e and speed ratio n, as shown in Fig. 8.

As can be seen from the figure, the removal error increased monotonically with the rising of the relative sampling interval. When eccentricity e and speed ratio n change to different combinations, the removal error curves show a little difference but the trend is the same. So it can be concluded that the removal error can be less than 10% in theory when relative sampling interval L' is no more than 0.2.

2. *Influence of the Removal Function Shape without Translation*

There are two factors that decided the removal function shape without translation: eccentricity e and speed ratio n. And the influence of them can be obtained through simulation, as shown in Fig. 9. The relative sampling interval $L' < 0.15$, the speed ratio range $n = 1$–10, eccentricity range $e = 0.5$–0.9, which basically cover the common range of dual-rotor processing parameters.

As can be seen in the figure, the removal error is increased monotonically with the rising of the speed ratio. When the speed ratio is low, the curve is steep, which shows the removal error is quite sensitive to the change of it. The eccentricity has great effect on the removal error, but this influence is complex. On the whole, when eccentricity is larger, the peak in the center of removal function is more prominent, which will lead to a larger removal error.

3. *Influence of Motion Velocity*

Here the motion velocity refers to the translation speed of the whole dual-rotor. However, simply considering the influence of motion velocity has little meaning, so the relative motion velocity can be defined as

$$V' = \frac{V}{v}, \tag{15}$$

where, V is the translation velocity of the whole dual-rotor, v is the orbital speed of the polishing head. Seen from the shape, the relative motion velocity V' actually characterizes the "stretch" level of the spiral path, and it also represents the ratio of the feed to the orbital radius in one orbital cycle. The simulation results are shown in Fig. 10.

In the figure, the removal error increases with the rising of the relative velocity V', but it does not increase monotonically, because the relative velocity does not directly affect the removal error. Seen between the curves, when relative sampling interval L' is larger, the error curve was significantly increased, showing the influence of the relative

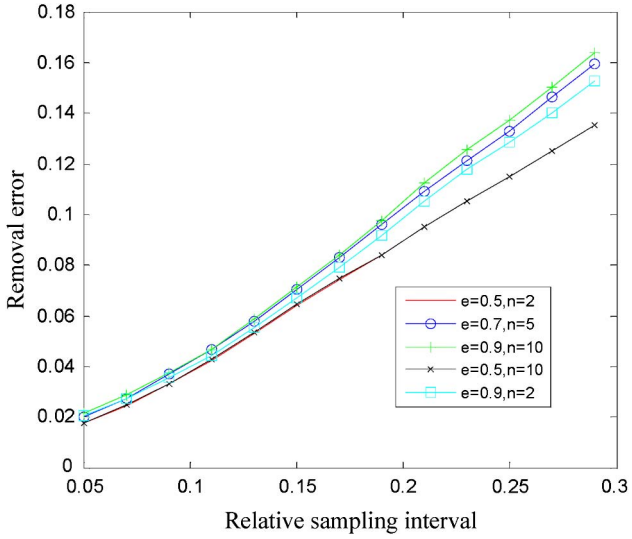

Fig. 8. Relationship between the relative sampling interval and the removal error.

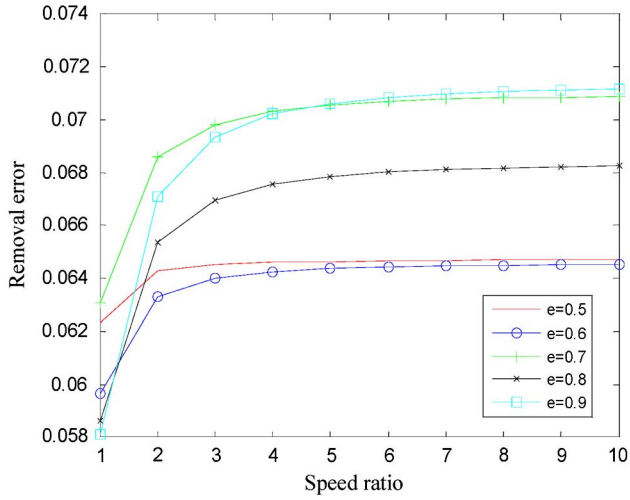

Fig. 9. Relationship between the removal function shape and the removal error.

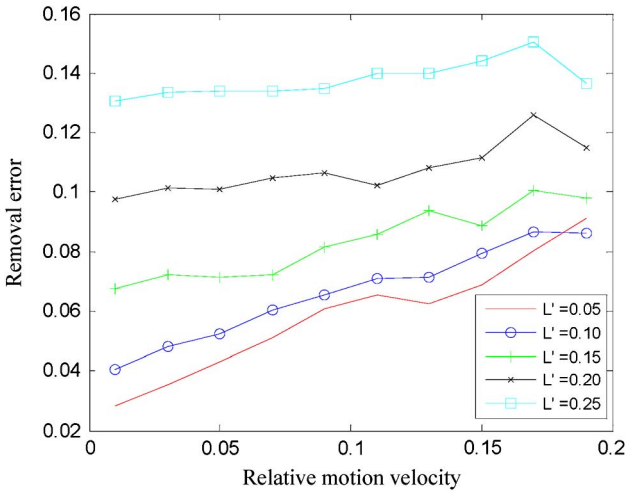

Fig. 10. Relationship between the relative motion velocity and the removal error.

sampling interval is greater than relative velocity, so an appropriate sampling interval should be selected first.

4. Experimental Results

In order to evaluate the dual-rotor tool path generation method and the effect of the AFP, a 100 mm diameter plane lens is selected as the workpiece, to make full aperture ultrasmooth processing experiment.

The processing parameters, which are shown in Table 1, can be selected according to the analysis in Subsection 3.C. As discussed above, the relative sampling interval L' should be chosen first and as small as possible in order to reduce the removal error. In the polishing process, the diameter of the removal function is usually fixed, so the actual sampling interval should be as small as possible. However, an extremely small sampling interval will lead to a sharp increase of the number of the resident points, which makes the solution of dwell time difficult. So considering the actual solving of the dwell time, the sampling interval is selected as $L = 2$ mm.

Then the removal function shape should be considered, which means to select the eccentricity e and the speed ratio n. In order to decrease the surface shape error effectively, the removal function should be similar to Gauss shape, and the parameter after optimization can be obtained from the literature [24] that the eccentricity e is 0.8, and the speed ratio n is 8. The diameter of the polishing head in the processing is 20 mm, so the diameter of the removal function is 36 mm, and the relative sampling interval L' is 0.056.

Table 1. Processing Parameters in AFP Experiment

No.	Parameters	Symbol	Value
1	Sampling interval	L (mm)	2
2	Relative sampling interval	L'	0.056
3	Eccentricity	e	0.8
4	Speed ratio	n	8
5	Orbital speed	v (mm/s)	3.5
6	Diameter of the removal function	D (mm)	36
7	The max relative motion velocity	$V'_{\max}$	0.094

The relative velocity has little effect on the removal error, so it is considered at last. In the processing, the translation velocity of the whole dual-rotor is decided by sampling interval and dwell time. In the solved dwell times, the shortest one is 0.105 min, so the speed can be calculated to be $V = 0.317$ mm/s, and that is the highest velocity in the polishing. So if the orbital speed v of the polishing head is faster than 3.17 mm/s, the relative speed V' can be guaranteed to be less than 0.1, and the removal accuracy will be ensured.

When processing parameters are fixed, the dual-rotor path can be generated. First, generate the raster scanning path according to the position of the dwell points. Then, like the process shown in Fig. 4, change the line section to dual-rotor path at each dwell point using the parameters in Table 1. At last, make the different dual-rotor path sections smooth, as discussed in Subsection 3.A. And the final generated dual-rotor path is shown in Fig. 11.

In order to validate the polishing effect of the dual-rotor path in the actual process, a Zygo interferometer is used for measuring the surface figure. The surface figure before processing is shown in Fig. 12(a). As can be seen, the surface figure before processing is 32.484 nm RMS, the middle is higher. Through solving of dwell time, the comparison of the surface figure between theory analysis and real processing is shown in Figs. 12(b) and 12(c). It can be seen that after processing, the figure accuracy is increased from 32.484 to 3.857 nm RMS. Seen from the appearance of the surface figure, the actual processing result is very similar to the theory one through careful design of process parameters. This experiment shows that the dual-rotor path can reduce the surface figure effectively.

In order to verify the smoothing effect of the ultrasmooth processing, the NewView 700 white-light

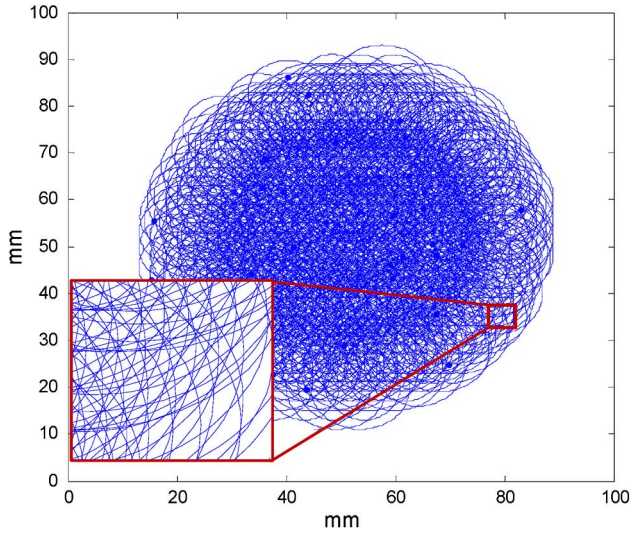

Fig. 11. Final generated dual-rotor path.

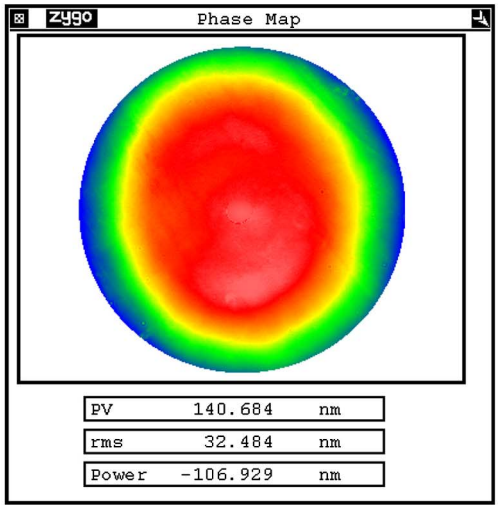

(a)

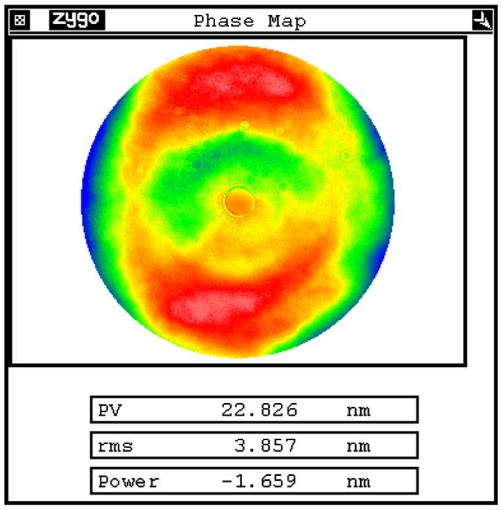

(b)

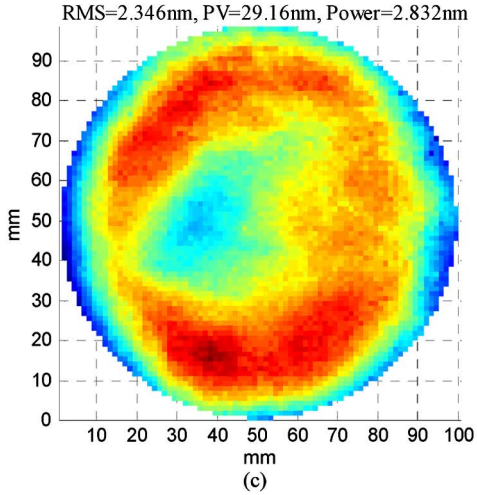

(c)

Fig. 12. Surface figures of the workpiece. (a) Before processing, (b) after processing, and (c) calculated in theory.

interferometer is used for measuring surface roughness. The comparison before and after processing is shown in Fig. 13. Before processing, the measured surface roughness of workpiece is typically 0.838 nm

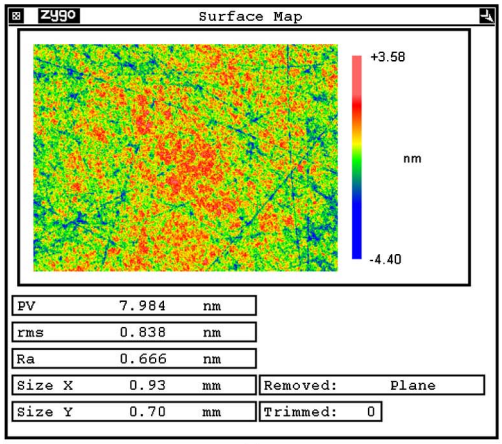

(a)

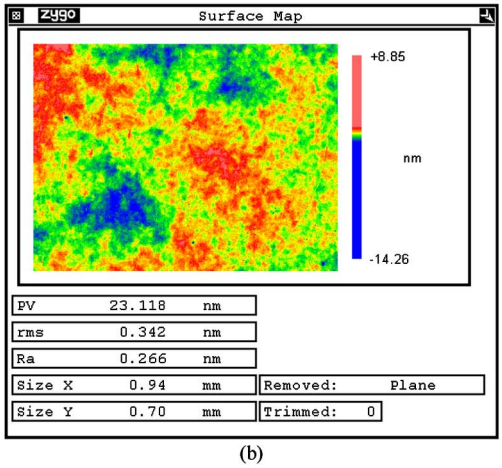

(b)

Fig. 13. Surface roughness of the workpiece. (a) Before processing and (b) after processing.

RMS, as shown in Fig. 13(a). As can be seen in the figure, there are a lot of random scratches on the original surface, which are the typical traces from rough processing. After processing, the typical surface roughness value is decreased to 0.342 nm RMS, as shown in Fig. 13(b). As can be seen, the random scratches before processing have disappeared, the surface undulation becomes gentle, so it proves to be a real ultrasmooth surface.

5. Conclusions

According to the characteristics of AFP technology, the method of the dual-rotor path is proposed to replace the complex dual-rotor polishing mechanism. The path is completely controlled by the machine, so it is simple to be generated and adjusted. Meanwhile, it improves the reliability and avoids the complicated works, such as mechanical design, machining, installation, and commissioning. The analysis results of removal error on the dual-rotor path show that, suitable process parameters can reduce the removal error to be small enough. Through experiment, the feasibility of dual-rotor path is validated, and the effectiveness of the AFP technology is also demonstrated. As can be shown, the AFP with

dual-rotor path can reduce the surface figure and roughness simultaneously.

The authors are grateful to their colleagues who cooperated to carry out the experiments and to their institution, the State Key Laboratory of Applied Optics. The research was funded by the key program of the major subject of national science and technology.

References

1. J. M. Bennett, J. J. Shaffer, Y. Shibano, and Y. Namba, "Float polishing of optical materials," Appl. Opt. **26**, 696–703 (1987).
2. H. Gao, J. Cao, and X. Chen, "Float polishing subnanometer-smooth surface," Acta Opt. Sin. **15**, 824–825 (1995).
3. J. V. Wingerden, H. J. Frankena, and B. A. V. der Zwan, "Production and measurement of superpolished surfaces," Opt. Eng. **31**, 1086–1092 (1992).
4. J.-D. Kim, "Motion analysis of powder particles in EEM using cylindrical polyurethane wheel," Int. J. Mach. Tools Manuf. **42**, 21–28 (2002).
5. M. Kanaoka, C. Liu, K. Nomura, M. Ando, H. Takino, Y. Fukuda, Y. Mori, H. Mimura, and K. Yamauchi, "Processing efficiency of elastic emission machining for low-thermal-expansion material," Surf. Interface Anal. **40**, 1002–1006 (2008).
6. Y. Mori, K. Yamauchi, K. Yamamura, H. Mimura, Y. Sano, A. Saito, K. Endo, A. Souvorov, M. Yabashi, K. Tamasaku, and T. Ishikawa, "Development of a figure correction method having spatial resolution close to 0.1 mm," Proc. SPIE **5193**, 105–111 (2004).
7. Z. Zhang, W. Liu, and Z. Song, "Particle size and surfactant effects on chemical mechanical polishing of glass using silica-based slurry," Appl. Opt. **49**, 5480–5485 (2010).
8. W. J. Choi, S. P. Jung, J. G. Shin, D. Yang, and B. H. Lee, "Characterization of wet pad surface in chemical mechanical polishing (CMP) process with full-field optical coherence tomography (FF-OCT)," Opt. Express **19**, 11343–11350 (2011).
9. L. D. Bollinger, G. Steiberg, and C. B. Zarowin, "Rapid optical figuring surfaces with plasma assisted chemical etching (PACE)," Proc. SPIE **1618**, 14–21 (1991).
10. D. W. Kim, S. W. Kim, and J. H. Burge, "Non-sequential optimization technique for a computer controlled optical surfacing process using multiple tool influence functions," Opt. Express **17**, 21850–21866 (2009).
11. S. F. Soares, D. R. Baselt, J. P. Black, K. C. Jungling, and W. K. Stowell, "Float-polishing process and analysis of float-polished quartz," Appl. Opt. **33**, 89–95 (1994).
12. Y. Namba and H. Tsuwa, "Mechanism and some applications of ultra-fine finishing," Ann. CIRP **27**, 511–516 (1978).
13. F. Preston, "The theory and design of plate glass polishing machines," J. Soc. Glass Technol. **9**, 214–256 (1927).
14. R. A. Jones, "Optimization of computer controlled polishing," Appl. Opt. **16**, 218–224 (1977).
15. R. A. Jones, "Grinding and polishing with small tools under computer control," Proc. SPIE **171**, 102–107 (1979).
16. R. A. Jones, "Fabrication using the computer controlled polisher," Appl. Opt. **17**, 1889–1892 (1978).
17. R. A. Jones, "Computer controlled polisher demonstration," Appl. Opt. **19**, 2072–2076 (1980).
18. R. A. Jones, "Computer controlled optical surfacing with orbital tool motion," Proc. SPIE **540**, 41–48 (1985).
19. R. A. Jones, "Computer-controlled polishing of telescope mirror segments," Opt. Eng. **22**, 222236 (1983).
20. J. R. Johnson and E. Waluschka, "Optical fabrication-process modeling-analysis tool box," Proc. SPIE **1333**, 106–117 (1990).
21. D. W. Kim and S. W. Kim, "Static tool influence function for fabrication simulation of hexagonal mirror segments for extremely large telescopes," Opt. Express **13**, 910–917 (2005).
22. A. Li, Y. Dai, Z. Zheng, and S. Li, "Study on removing function of the polishing pad of dual—rotator mechanism," Chin. Mech. Eng. **15**, 2077–2081 (2004).
23. Y. Dai, W. Shang, and X. Zhou, "Effection of the material of a small tool to the removal function in computer control optical polishing," J. Natl. Univ. Defense Technol. **28**, 97–101 (2006).
24. X. Chen, P. Guo, and J. Ren, "Optimization of removal function in computer controlled optical," Proc. SPIE **7655**, 76551Y (2010).